The bolometer diagnostic at the stellarator Wendelstein 7-X

P. Hacker[1,2], D. Zhang[1], R. Burhenn[1], B. Buttenschön[1], T. Klinger[1], and the W7-X Team[1]

[1]Max Planck Institute for Plasma Physics, Wendelsteinstr. 1, D-17491 Greifswald, Germany
[2]Ernst-Moritz-Arndt University Greifswald, Domstr. 11, D-17489 Greifswald, Germany

Bolometer

Goals

- to investigate total radiation powerloss through impurities and its distribution
- global/local power balance, as well as (later) impurity and transport studies through tomographic inversion

Performance

- multi-device system: horizontal bolometer camera (HBC, 32 channels) and vertical bolometer camera (VBC, 20 channels for each of two subdetectors)
  $\Rightarrow$ more detectos with different filters/coatings available, e.g. for investigation of soft x-ray radiation
- VBC/HBC detector arrays with carbon coated, 5 µm thick gold-foil absorbers for maximum absorbtion at sensitivity of 200 nW and minimum reflectivity (visible light to SXR between 600 nm to 0.2 nm)
- fan-shaped lines of sight provide full plasma coverage at 5 cm spatial resolution
- Au-foil on 7.5 µm SiN substrate, backed by a gold meander with 0.25 ms response time due to thermal diffusion
- temporal resolution in range of 0.08 ms to 1.6 ms, depending on experiment and data economy

Design Criteria

- steady state operation at discharges with up to 30 min of 10 MW heating power ensured by cooling system with graphite elements and water cooling structures
- impact of electron cyclotron resonance heating (ECRH) stray radiation (several 10 kW m^{-2} at 140 GHz) reduced by a conductive wire-mesh of thickness 90 µm and 0.24 mm spacing in front of the detector array, as well as a ceramic TiO/Al_2O_3 coating inside the camera housing
  $\Rightarrow$ 3% microwave transmission, optical transmission factor 53%

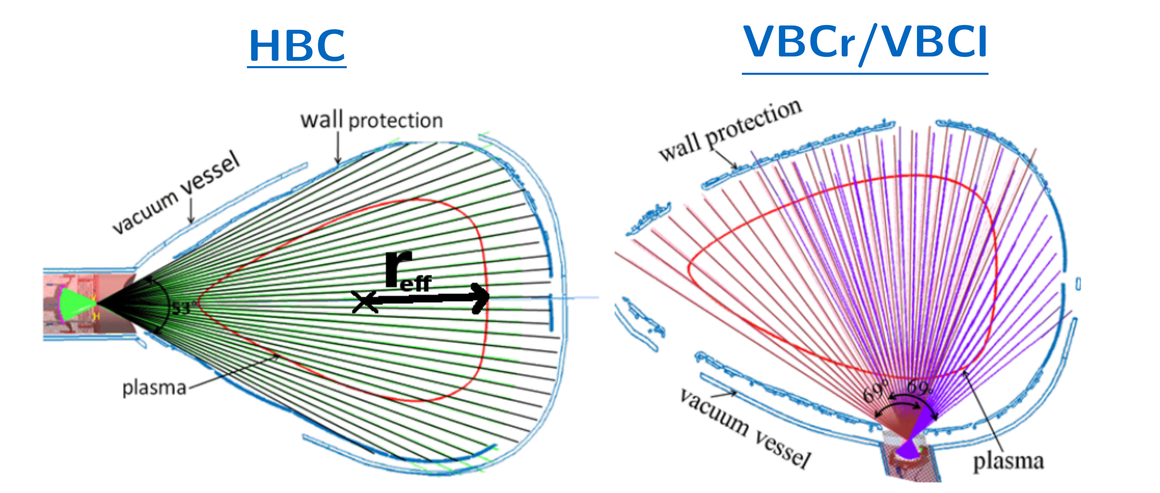

Lines of sight for HBC (32 channels) and VBC (two 20-channel subdetector arrays) with individual apertures, retracted into the vacuum vessel behind protective wall elements. Located in the triangle-shaped plane at W7-X.[1]

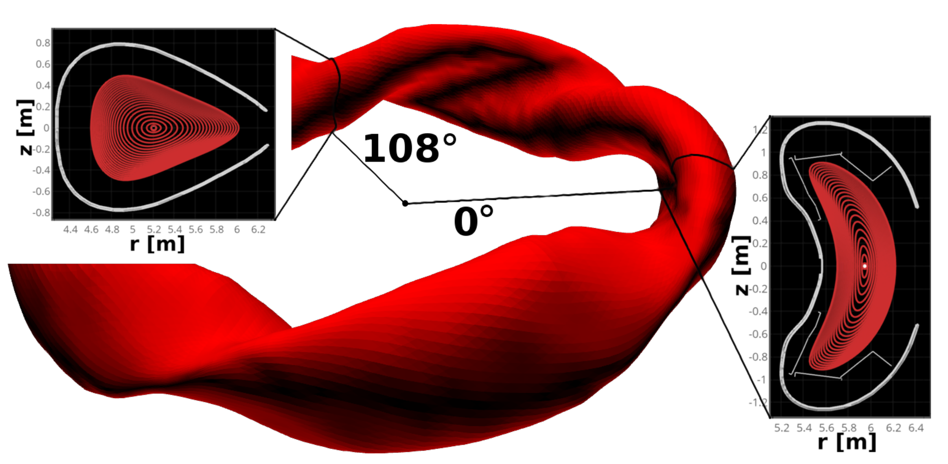

W7-X plasma vessel (torus, center) with equilibrium fluxsurfaces (red), calculated by VMEC[4] at triangle- (top-left, 108°) and "*bean*"-shaped (bottom-right, 0°) planes.

Components

Camera Head Construction

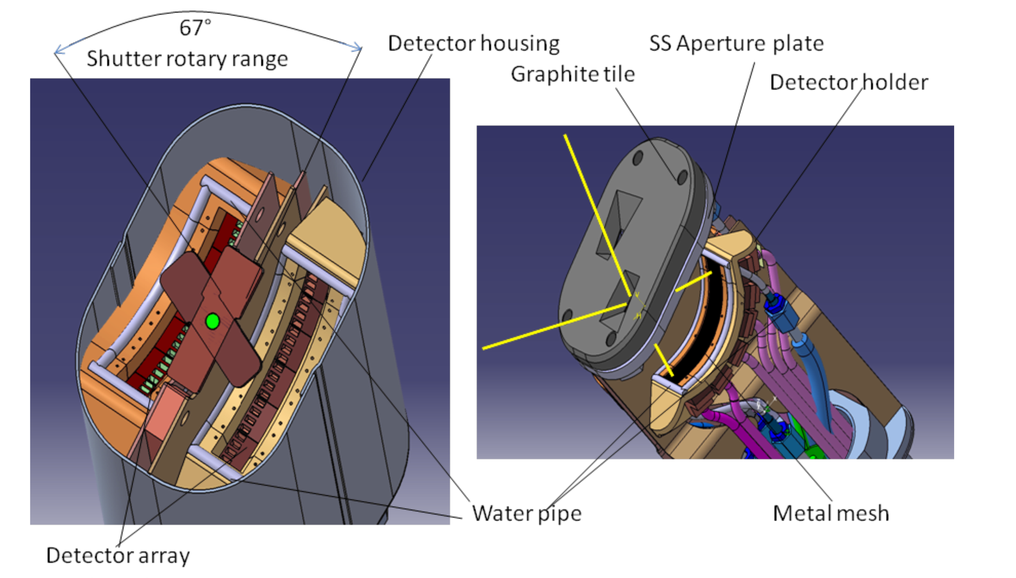

Camera head (VBC) construction. Subdetector arrays on water cooled holdings with optic baffles (left). Capped graphite tile with stainless steel aperture for thermal protection.[1]

Detector

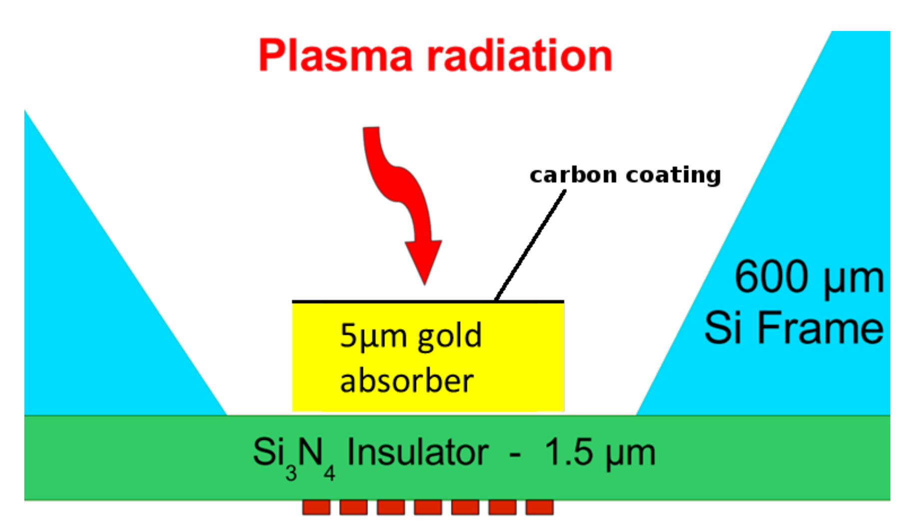

Scheme of a single detector channel with housing/holder, absorption foil, substrate and meander.[7]

References

[1] "Design Criteria of the Bolometer diagnostic for steady-state operation of the W7-X stellarator"; Zhang, D. et al.; Review of Scientific Instruments, Jan 1st, 2010; DOI:10.1063/1.3483194

[2] "The bolometer diagnostic at stellarator Wendelstein 7-X and its first results in the initial campaign"; D. Zhang, et al. and the W7-X Team; Stellarator-New 2017

[3] "A low noise highly integrated bolometer array for absolute measurement of VUV and soft x radiation"; K. F. Mast et. al; Review of Scientific Instruments 62, 744 (1991); DOI: 10.1063/1.11.42078

[4] "Steepest descent moment method for three dimensional magnetohydrodynamic equilibria"; Hirshman, S.P. et al.; Physics of Fluids 26, 3553, (1983); DOI: 10.1063/1.864116

[5] "Tokamaks"; Wesson, J.; Clarendon Press, Oxford; 1987

[6] "Numerical investigation of plasma edge transport and limiter heat fluxes in Wendelstein 7-X startup plasmas with EMC3-EIRENE"; Effenberg, F., Feng, Y. et al. Nucl. Fusion 57 (2017) 036021 (15pp); DOI: 10.1088/1741-4326/aa4f83

[7] "Derivation of bolometer equations relevant to operation in fusion experiments"; Gianone, L. et al.; Review of Scientific Instruments; 20th of November, 2002; DOI: 10.1063/1.1498906

[8] "Results of the bolometer diagnostic at OP 1.a of W7-X"; internal review of the physics plan during the second operational phase at the stellarator W7-X; 28.02.20i18

[9] "Characterization of energy confinement in net-current free plasmas using the extended International Stellarator Database"; H. Yamada et al.; INSTITUTE OF PHYSICS PUBLISHING and INTERNATIONAL ATOMIC ENERGY AGENCY; Nucl. Fusion 45 (2005) 1684¿1693

Calibration

- *in-situ calibration* when ultra-high vacuum pneumatic shutter is closed before every experiment
- reference correlation with un-exposed, indentical part of the detectors *Wheatstone bridge* with two calibration gold-foils of same thickness and size
- for each channel, calibration is performed by a 5 W pre-heating with closed shutter, regarding cooling time, capacity and resistance[7]
  $\Rightarrow$ temperature change in Au film leads to change in resistance of underlying gold meanders

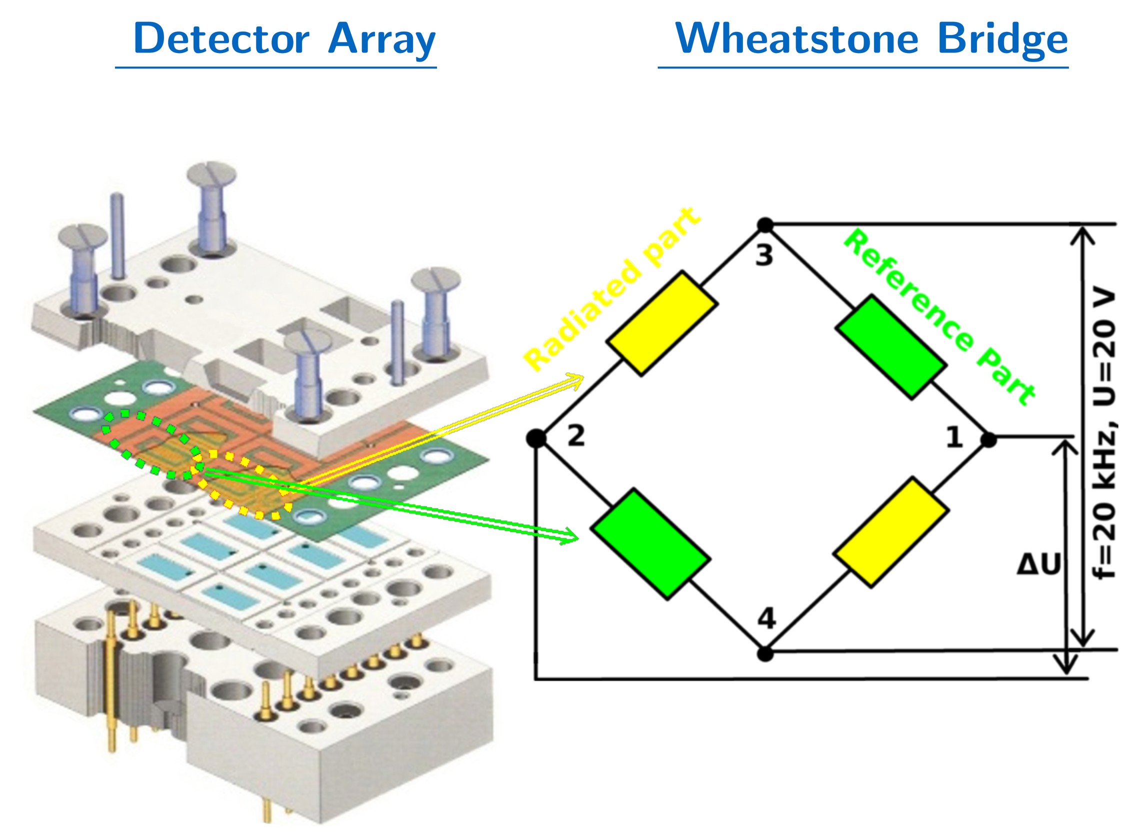

(Left) Detector array with sealed reference array, meander and holder. (Right) Wheatstone bridge with radiated part (yellow) and reference (green), left un-exposed throughout operation. Reference and measurement resistances of the foils are the same.[7]

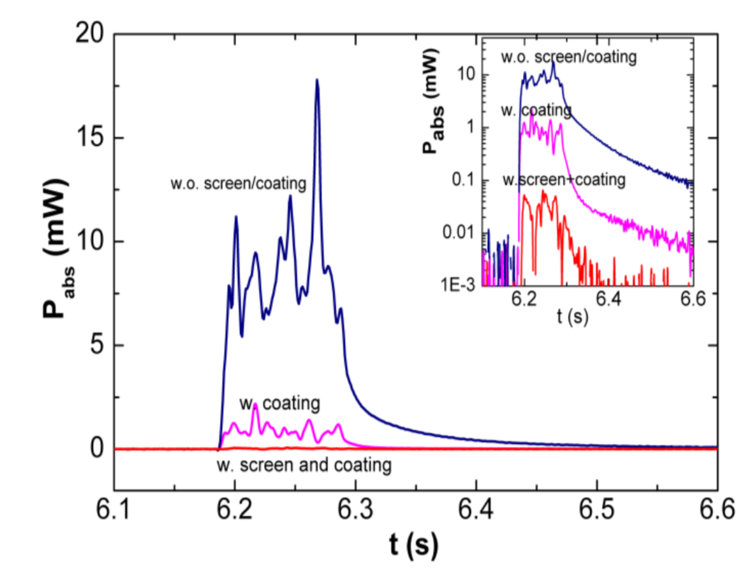

Test results of a bolometer prototype in a strong microwave background provided by MISTRAL[2] with an withouth microwave suppresion measures (see left).

Results

Equations

The radiation power observed by the bolometers equals to:

$$P_{rad,bolo} \propto \sum_Z n_e \cdot n_Z \cdot L_Z$$

where L_Z is the line radiation function by impurities (Z):

$$L_Z = f\left(T_e, T_i, T_Z, wall\ material/conditions,\ \dots\right)$$

For each channel the observed power P_{Ch} can be calculated by using:

$$P_{ch} = \frac{2}{V_{eff}} \cdot (R_{ch} + 2R_C) \cdot \kappa_{ch}\sqrt{g_C} \cdot \left(\tau_{ch}\frac{\mathrm{d}(\Delta U)}{\mathrm{d}t} + f_\tau \cdot (\Delta U)\right) \qquad (1)[7]$$

with $\Delta U \propto \Delta T$ the change in measurement voltage and absorber temperature

- properties denoting $(\cdot)_{ch}$ are the individual channel/foil characteristics, e.g. cooling time (τ), heat capacity (κ) and resistance (R)
- R_C and C_{cab} are the connection cable resistance and capacity with 41 Ω and 9 nF respectively
- f_{Bridge} is a dimensionless scaling factor of the Wheatstone bridge

Global Power Estimate: for each camera (VBC, HBC) individually

$$P_{rad} = \frac{V_{P,tor}}{V_{cam}} \cdot \sum_{ch} \frac{V_{ch}}{K_{ch}} \cdot \frac{P_{ch}}{53\%} \qquad (2)$$

with:

$$V_{cam} = \sum_{ch} V_{ch}$$

- V_{ch} the volume of the polygon created by the lines of sight of each detector and the corresponding aperture $\Rightarrow V_{cam}$ is the total volume investigated by the camera
- P_{ch} is calculated via eq. (1)
- scaling with 53% due to the reduced input intensity of the stray radiation wire mesh
- $V_{P,tor}$ the estimated plasma volume from which radiation is emitted, approximated using one field configuration in an EMC3-Eirene simulation

quasi-steady state

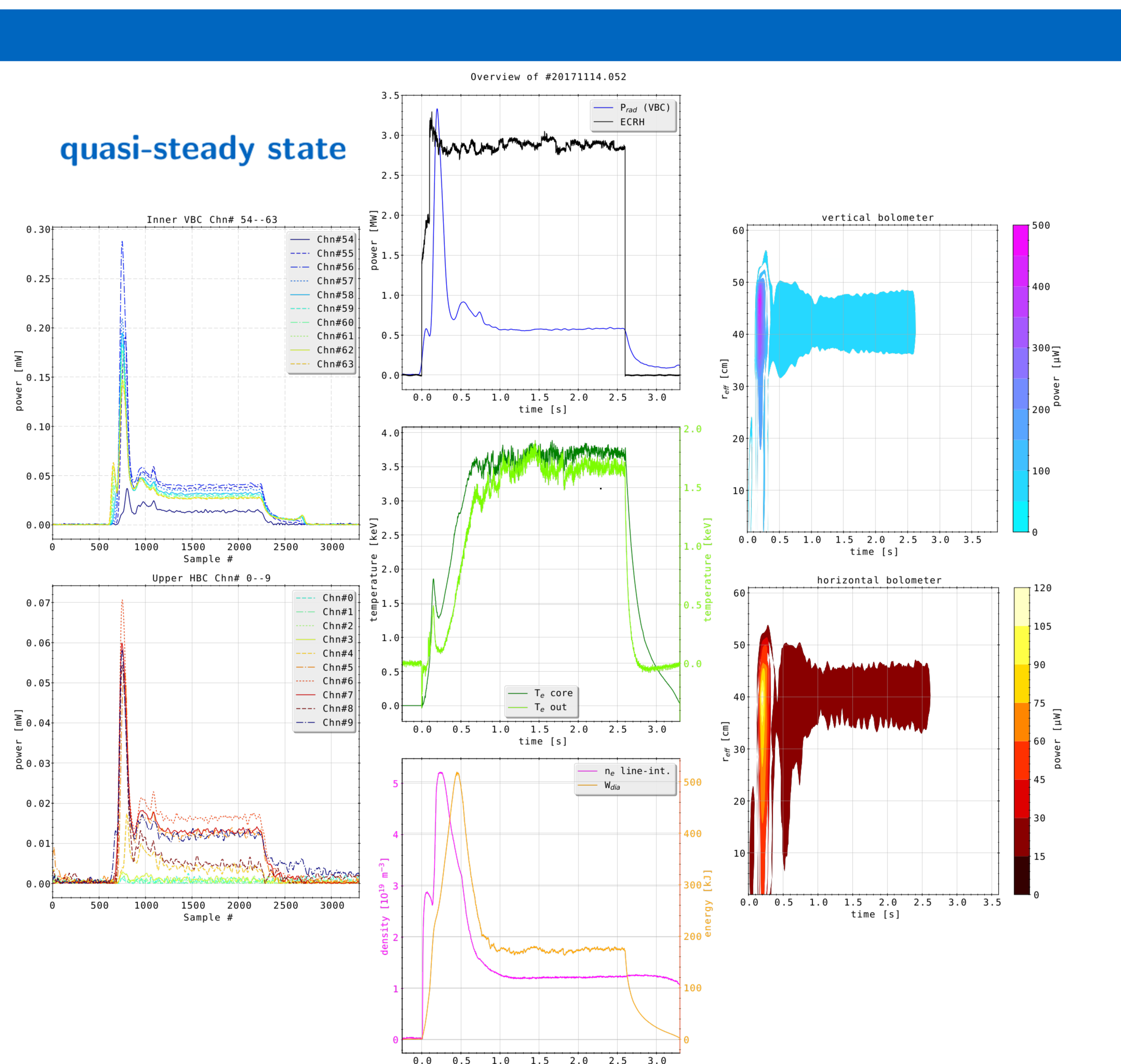

XP.20171114.052: (LEFT) Calculated powers from eq. (1) for the inner-/uppermost channels from the VBC/HBC. One sample equals 1.6 ms. A *Savitzky-Golay* filter with a 31 sample window is used on both raw signal/derivative to minimize bitwise noise from the A2D converter. (MIDDLE) Experiment parameters for the same discharge (2.7 s, terminated). (RIGHT) channel power vs. effetive plasma radius, e.g. $\rho_{eff} = \sqrt{\Psi_N}$ the distance from the magnetic field center, for both camera.

radiative collapse

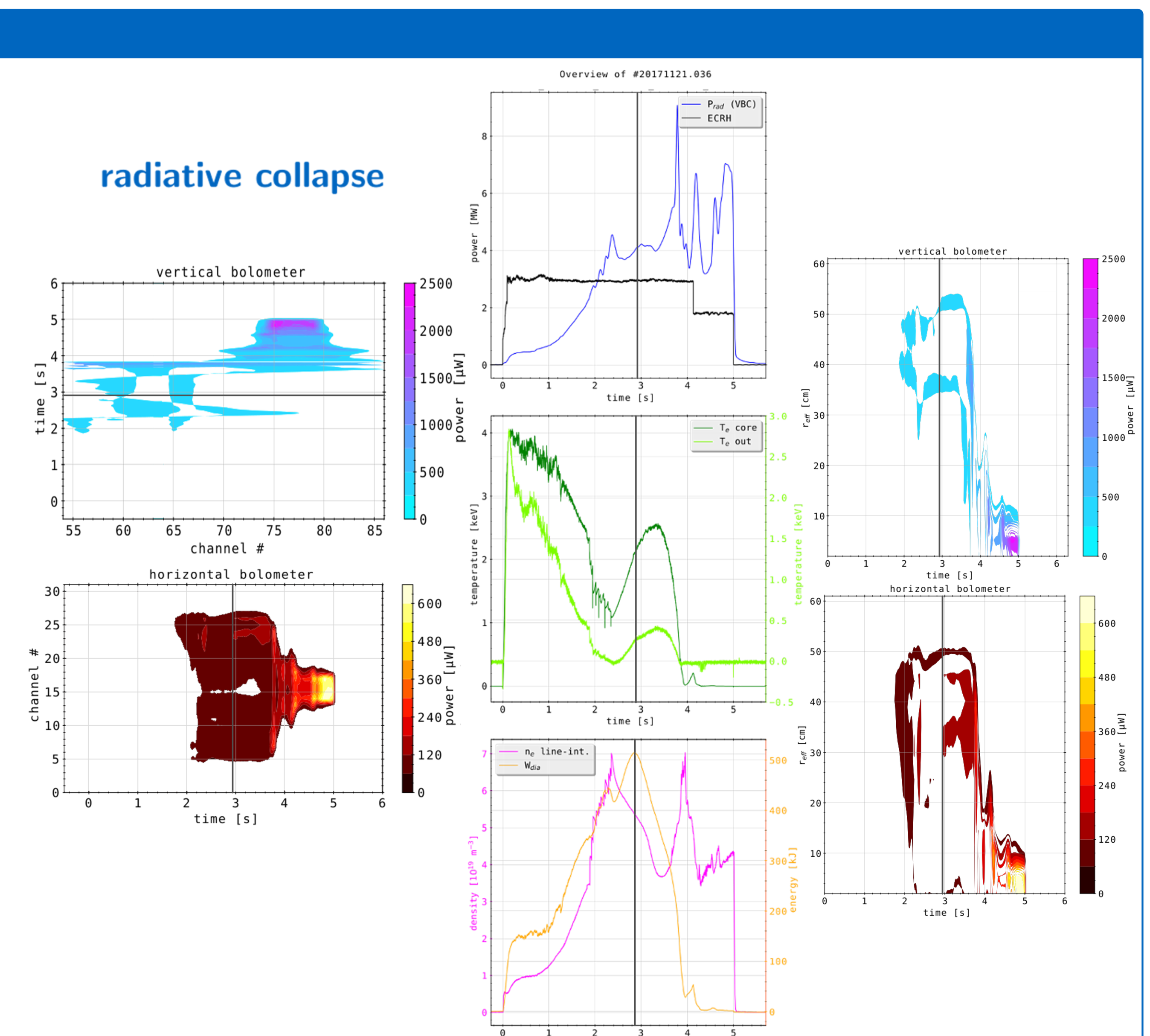

XP.20171121.036: (LEFT) Channel number vs. power, e.g. the center corresponds to the center of the plasma core. (MIDDLE) The most important discharge properties. Similar setup as for the left discharge, but with forward feeding by frozen H_2 pellet injection. The discharge collapses where the stored, diamagnetic energy in the plasma drops drastically around 2.9 s. P_{rad} shows that this corresponds to a radiative collapse, where the plasma shrinks towards the magnetic axis (as seen in the left figures), and all the input and stored energy is irradiated. (RIGHT) The channel power over the effective plasma radius.

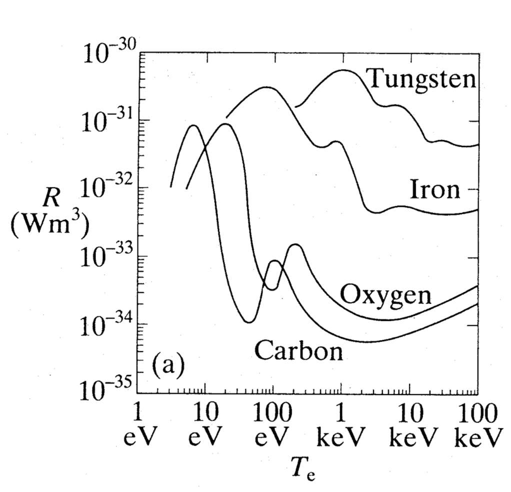

Impurity radiation intensities for most relevant elements in the device. Carbon and, but most importantly oxygen impurity radiation is assumed to contribute the most to line radiation.[5]

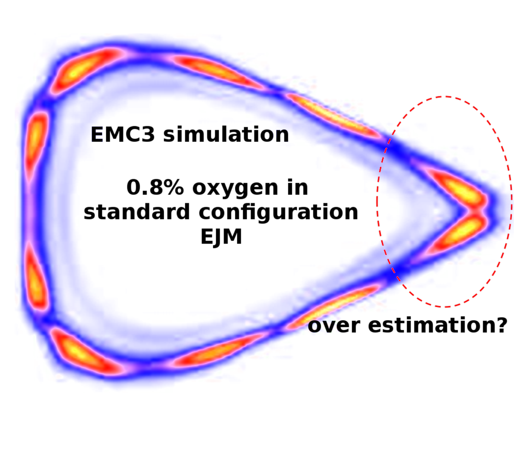

EMC3-Eirene simulation results, which show the relative radiation profile/emissivity for 80% oxygen impurities beyond the last closed fluxsurface (LCFS).[6]

Conclusion

- high-density, high-radiation discharges can show
  $$f_{rad} = \frac{P_{rad}}{P_{ECRH}} \approx 1$$
- inboard and lower plasma regions irradiate more intense in EJM magnetic field configuration
- steady state: mainly radiation from outer plasma regions/LCFS
- radiative collapse: strong centrification of plasma source (see r_{eff}, core very bright)
- after W_{dia} the plasma-stored energy begins to decrease, discharge has already begun to collapse and the input power is irradiated, hence $f_{rad} \geq 1$
- collapse likely triggered around $t \approx 2.3$ s, by first pellet injection - edge localized radiation? -, causing the plasma to shrink
- in radiative collapse case: thermal instabilities (see T_e) triggered around plasma edge
  $\Rightarrow$ local events, causing effective cooling by increasing P_{rad}
- however, operational phase 1.2a (OP1.2a) at W7-X showed possible high-performance discharges with great power-exhaust capabilities around LCFS/scrape-off-layer
  $\Rightarrow$ detachment with plasma shrinkage, less impurity, better wall conditioning ...

OP1.2a

Collected database of different discharge setups/characteristics where radiation fraction reached unity. Results based on Yamada et al.[9] show good agreement for the energy confinement time scaling for: [8]

$$\tau_{E,ISS04} \propto n_e^{0.54}$$

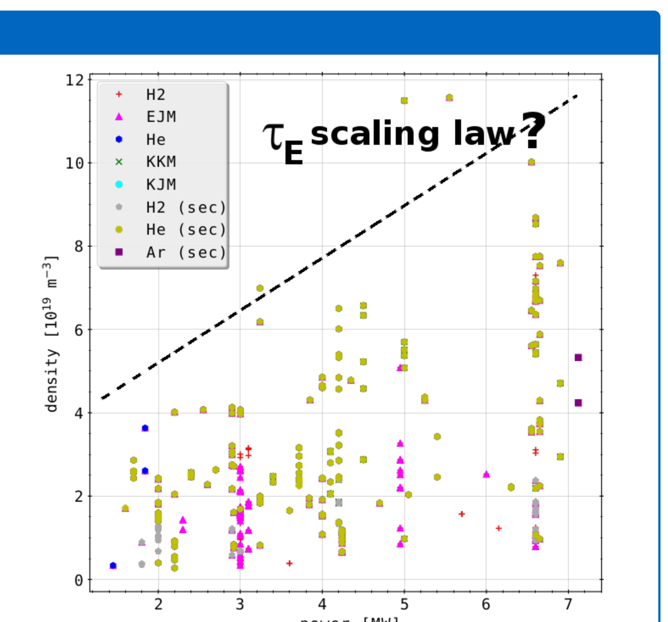

82. Jahrestagung der DPG und DPG-Frühjahrstagung der Sektion AMOP, Erlangen, 04.03. - 09.03.2018

Authors correspondence: P. Hacker, philipp.hacker@ipp.mpg.de; D. Zhang, daihong.zhang@app.mpg.de

EUROfusion

This work has been carried out within the framework of the EUROfusion Consortium and has received funding from the Euratom research and training programme 2014-2018 under grant agreement number 633053. The views and opinions expressed herein do not necessarily reflect those of the European Commission.